Article

J. Biol. Regul. Homeost. Agents. 2024; 38(5): 3919–3934
https://doi.org/10.23812/j.biol.regul.homeost.agents.20243805.310

Chitosan Nanocapsules Boost Capsaicin's Efficacy against Diabetes-Induced Cardiotoxicity in Rats

Rasha A. Mansouri[1,*]

[1]Department of Biochemistry, Faculty of Sciences, King Abdulaziz University, 22254 Jeddah, Saudi Arabia
*Correspondence: amansouri@kau.edu.sa (Rasha A. Mansouri)
Published: 1 May 2024

Background: Capsaicin is known for its therapeutic benefits, including anti-inflammatory, antioxidant, and cholesterol-lowering effects. However, its clinical application is limited by poor bioavailability, primarily due to its low solubility in water.
Objective: To evaluate the efficacy of our newly optimized capsaicin-loaded chitosan nanocapsules (CAP@CS) in mitigating cardiotoxicity induced by type 2 diabetes mellitus (T2DM) and a high-fat diet in male Sprague Dawley rats.
Methods: Nanocapsules containing capsaicin and chitosan were synthesized using the micro-emulsion technique and characterized using dynamic light scattering (DLS) and transmission electron microscopy (TEM), were administered to sixty male rats, which assigned to five groups: control, diabetic, diabetic with rosuvastatin, diabetic with capsaicin (CAP), and diabetic with CAP@CS. The inflammatory markers and biochemical indicators associated with myocardial damage, tissue oxidative stress, and inflammation were assessed.
Results: DLS analysis revealed an average size of ~260 nm and a zeta potential of ~+18 mV. TEM images depicted circular and uniform nanocapsules. The diabetic + CAP@CS group showed more significant reductions in blood glucose and lipid levels compared to other diabetic groups, and markedly increased the concentrations of the antioxidant enzymes superoxide dismutase (SOD), catalase, and glutathione peroxidase (GPx), reduced glutathione, and upregulated nuclear factor erythroid 2-related factor 2 (NRF-2), and heme oxygenase-1 (HO-1) expressions more significantly than the diabetic + CAP group. CAP@CS upregulated nitric oxide concentrations and its bioregulator, inducible nitric oxide synthase (iNOS), demonstrating enhanced cardioprotection. The formula exhibited a more pronounced anti-inflammatory impact, as demonstrated by the tumor necrosis factor-alpha (TNF-α), interleukin-6 (IL-6), and interleukin-1 beta (IL-1β) assessment. Histological investigations employing hematoxylin and eosin stain, Masson trichrome (MTC), and immunohistochemical analysis of α-smooth actin and desmin revealed the notable superiority of the new formula (CAP@CS) over capsaicin (CAP) in mitigating the myocardial damage mediated by diabetes. This efficacy was substantiated by assessments of myocardial protein content, malondialdehyde (MDA), heat shock protein 70 (HSP70) determination, alanine transaminase (ALT), aspartate transaminase (AST), and troponin levels.
Conclusion: CAP@CS nanocapsules present a promising therapeutic strategy, improving for cardioprotection in T2DM, offering potential benefits such as improved efficacy, bioavailability, and reduced side effects.

Keywords: capsaicin; type 2 diabetes; cardiotoxicity; chitosan nanocapsules; cardioprotection; high-fat diet

Introduction

Diabetes mellitus encompasses diverse metabolic disorders marked by a chronic elevation of blood glucose levels. Individuals with diabetes face an elevated risk of severe health complications, resulting in heightened medical costs, reduced quality of life, and increased mortality [1]. Persistent hyperglycemia adversely affects the vascular system, causing damage to the heart, eyes, kidneys, and nerve blood vessels, ultimately leading to life-altering complications [2].

In diabetic patients, oxidative stress has been established as a primary contributor to the onset of cardiomyopathy and myocardial structural changes in the myocardium, leading to the progression of cardiac failure. Pathological hypertrophy is characterized by cardiomyocyte enlargement, along with the presence of cardiac fibrosis and apoptosis in the myocardium, induced by oxidative stress factors [3–5]. Additionally, oxidative stress can induce cardiac fibrosis by increasing collagen production, promoting the conversion of fibroblasts to myofibroblasts, and stimulating the production of transforming growth factor-β [6]. Conversely, interleukin-1 beta (IL-1β) and IL-6, along with tumor necrosis factor-alpha (TNF-α), have been identified as contributors to the progression of cardiomyopathy and dysfunction in diabetics. Genetic disruption of these cytokines positively impacted a mouse model, decreasing hypertrophy, fibrosis, and cardiac dysfunction. Molecular mechanisms implicated in myocardial inflammation in diabetes encompass activation of the NF-κB pathway, leading to upregulation of cytokines, chemokines, and adhesion molecules, thereby contributing to cardiomyopathy [3,7].

Journal of
BIOLOGICAL REGULATORS
and Homeostatic Agents

Chitosan nanoparticles (CS) are increasingly recognized as a versatile platform for innovative drug delivery systems due to their favorable properties, such as biodegradability, biocompatibility, enhanced stability, minimal toxicity, and ease of preparation [8]. Various therapeutic agents, including small molecules, proteins, and polynucleotides, can be encapsulated within chitosan nanoparticles [9–12].

Capsaicin (CAP), the primary natural alkaloid found in chilies and peppers, demonstrates diverse therapeutic potential, encompassing analgesic [13], anti-inflammatory [14], anti-cancer [15], bactericidal [16], and antioxidant properties [17]. The clinical application of CAP is hindered by its low aqueous solubility and limited bioavailability, reducing therapeutic efficacy. Therefore, the imperative is the development of new strategies to improve the CAP's solubility and bioavailability [18]. Researchers have explored innovative delivery systems [19]. These include micro- and nano-emulsions [20,21], liposomes [22], micelles [23], hydrogel beads [24], and solid nanoparticles [25].

This study aimed to enhance the efficacy of CAP against cardiac myopathy in type 2 diabetes mellitus (T2DM) by developing stable capsaicin-loaded chitosan nanocapsules (CAP@CS). The CAP@CS were prepared using the micro-emulsion method and characterized by particle size, zeta potential analysis, and transmission electron microscopy (TEM). Their therapeutic effectiveness in mitigating myocardial damage was investigated in a T2DM animal model. Myocardial redox status was assessed through malondialdehyde (MDA), antioxidant enzyme activity (SOD), and serum levels of inflammatory cytokines (TNF-α, IL-6), liver enzymes (aspartate transaminase (AST), alanine transaminase (ALT)), and nitric oxide (NO). Additionally, histopathological examinations of myocardial tissues were performed in normal, diabetic, and diabetic-treated animals.

Materials and Methods

Materials

CAP (M2028, purity ≥95%), low-viscous chitosan (#50494), potassium phosphate monobasic anhydrous (#795488), sodium phosphate dibasic dihydrate (#P7751), sodium acetate (#S8750), acetic acid (#506007), polyethylene glycol (#8.17045), glucose (#1724615), tween 80 (#655207) methanol (#1098229), and citrate-phosphate buffer (#P4809) were purchased from Sigma-Aldrich (St. Louis, MO, USA).

Preparation of CAP@CS Nanocapsules

Capsaicin-loaded chitosan nanocapsules (CAP@CS) were synthesized using the previously described micro-emulsion method [26] with some modifications. The oil phase was prepared by dissolving 5 mg CAP in 200 mL of absolute ethanol containing 1 mg/mL polyethylene glycol (molecular weight 6000). Concurrently, an aqueous phase comprising 10 mg chitosan in 20 mL of a 1% (v/v) acetic acid solution was stirred at room temperature. These two phases were combined and stirred for 2 hours to form a stable oil-in-water (O/W) micro-emulsion. To eliminate uncaptured CAP, the mixture underwent dialysis against a phosphate buffer (pH 8.5) for 12 hours using a dialysis bag. This procedure resulted in the formation of the final CAP@CS nanocapsules.

Physicochemical Characterization of CAP@CS

The particle size, surface charge (zeta potential), and size distribution of CAP@CS nanocapsules were determined using dynamic light scattering (DLS) on a ZetaSizer Nano (Malvern Instruments Ltd., Bristol, UK). Each sample was measured three times, and the reported values represent the average. The dispersity of particle sizes was quantified by the polydispersity index (PDI). Additionally, a transmission electron microscope (LEO 906 E, Carl Zeiss Microscopy GmbH, Jena, Germany) provided visual confirmation of the size and surface features of the synthesized CAP@CS nanocapsules.

The entrapment efficiency (EE) of CAP into the CAP@CS was estimated, where, nanocapsules were centrifuged at 20 °C. The supernatant, containing any free CAP, was collected after centrifugation. A UV-Vis spectrophotometer (UV-1601, Shimadzu, Kyoto, Japan) measured the amount of unencapsulated CAP at its maximum absorption wavelength of 280 nm. Entrapment efficiency (EE) of CAP within the nanocapsules was then calculated using the following equation:

$$EE(\%) = [(T - C) / T] \times 100$$

Where T represents the initial total amount of CAP added and C represents the free CAP concentration in the supernatant. All experiments were performed in triplicate.

In Vitro Release of CAP from CAP@CS

The release profiles of capsaicin-loaded chitosan nanocapsules (CAP@CS) and free CAP were compared *in vitro* using a dialysis method. Two pH environments (pH 4 and 7.4) were investigated. Release experiments were conducted with an NE4-COPD dissolution test apparatus (Copley Scientific, Nottingham, UK). In brief, 5 mL of the prepared nanocapsule suspension was placed in a dialysis bag, immersed in 900 mL of the selected release medium at 37 ± 0.5 °C, and stirred at 100 ± 2 rpm. At predefined time intervals, 3 mL of the dissolution medium was withdrawn and replaced with fresh medium. The released CAP concentration was measured at each point by monitoring the absorbance peak at 280 nm using a UV-Vis spectrophotometer (UV 1601, Shimadzu, Osaka, Japan).

Mathematical Modeling and Release Kinetics

To ascertain the most appropriate model describing the CAP's dissolution profile, *in vitro* dissolution data were analyzed using various kinetic models, including zero-order [27], first-order [28], Higuchi diffusion [29], Korsmeyer-Peppas [30], Hixon-Crowell [31], and Weibull [32]. Model selection for fitting the release data was determined by the correlation coefficient R^2 within the previously described models. The model producing the highest R^2 value was considered to provide the most accurate representation of the release data.

Stability Studies

To evaluate the formulation's stability, samples were stored at both 4 °C and room temperature. Particle size, polydispersity index (PDI), and zeta potential were measured at predetermined intervals, including upon fresh preparation and after 4 weeks of storage. All measurements were performed in triplicate.

Animals and Experimental Design

Animals

Sixty male Sprague-dawley rats weighing 130–140 grams were housed in well-ventilated, lit, top-opening cages with free access to water and food. They were maintained at a temperature of 26 ± 3 °C and subjected to a 12-hour light-dark cycle. The study protocol received approval from the Standing Committee of Bioethics Research (Approval No. 222/2024) at Prince Sattam Bin Abdulaziz University.

After a ten-day acclimatization period, the animals underwent an 8-hour fast, followed by a single intraperitoneal (i.p.) administered dose of streptozotocin (STZ) at a dose of 40 mg/kg, dissolved in a citrate-phosphate buffer (pH 4.5). The control group received an i.p. injection of citrate-phosphate buffer alone and followed a standard diet for two weeks.

Diabetic categorization was established when fasting blood glucose exceeded 250 mg/dL at 48 h after STZ i.p. administration, as confirmed by an oral glucose tolerance test (OGTT) conducted by an ACCU-Chek Active (Roche Diagnostics) glucometer. The OGTT, performed two weeks after STZ injection on two different days, assessed blood glucose levels at fasting, 30, 60, 90, and 120 min after oral intake of a 40% glucose solution (3 g/kg). Rats with OGTT levels surpassing 11.1 mmol/L were considered diabetic, and only uniformly hyperglycemic rats were included for subsequent investigations [33].

The diabetic group was fed a high-fat diet (HFD) consisting of 25% protein, 17% carbohydrate, and 58% fat as a percentage of total calories.

Experimental Groups

(1) Control group: Animals received a daily 1% Tween-80 suspension (1 mL/kg, p.o.) dissolved in distilled water for 12 weeks.

(2) Diabetic group: Animals, in addition to a high-fat diet (HFD), were orally administered a daily 1% Tween-80 suspension (1 mL/kg, p.o.) dissolved in distilled water for 12 weeks.

(3) Rosuvastatin-treated group: Animals on HFD were orally administered rosuvastatin (R148P0, Sigma-Aldrich, St. Louis, MO, USA) at 20 mg/kg/day for 12 weeks [34].

(4) CAP-treated group: Animals on an HFD were orally administered CAP (Sigma-Aldrich, St. Louis, MO, USA) at a 6 mg/kg/day dose for 12 weeks [35].

(5) CAP@CS-treated group: Animals on HFD orally received CAP@CS nanocapsules (6 mg/kg/day) for 12 weeks.

Throughout the experiment, animal weights and fasting blood glucose were monitored weekly, and treatment doses were adjusted according to their weights. One week before concluding the study, rats underwent an overnight fast, and the oral glucose tolerance test (OGTT) was performed in triplicate.

Upon study completion, rats were fasted for 12 hours overnight and sacrificed under ketamine anesthesia (50 mg/kg, i.p.). Blood was collected from the inferior vena cava and centrifuged at 3000 rpm for 15 min, and the collected serum was refrigerated at –20 °C for future biochemical analysis. Hearts were promptly dissected and washed with cold saline (4–6 °C), and portions of the cardiac tissues were collected from all groups. These tissues were homogenized in a cold potassium phosphate buffer solution (100 mM), centrifugation at 3000 rpm for 20 minutes to obtain a 10% concentration homogenate, followed by supernatant collection, and stored at –80 °C for further analysis.

Histopathological Analysis

Hematoxylin and Eosin (H&E) Staining

The heart muscles of the collected rats were fixed in 10% formalin for 24 hours at 28–27 °C. Subsequently, the muscles were embedded in wax and sliced into five-micrometer-thick sections. Sections of the myocardium underwent staining by H&E following standard procedures, involving a five-minute exposure to 0.8% hematoxylin (RBA-4213-00A, CellPath, Powys, UK) and a three-minute application of 0.35% eosin stain (RBC-0201-00A, CellPath, Powys, UK) at 28 °C. Tissue structures were examined by an Olympus BX53 (Olympus, Tokyo, Japan) light microscope at 200× magnification. The severity of myocardial damage was graded as follows: 0 = Normal tissue without changes, 1 = mild multifocal damage with mild inflammation, 2 = moderate myocardial damage and/or ad-

Journal of
BIOLOGICAL REGULATORS
and Homeostatic Agents

vanced inflammatory infiltration, 3 = advanced myocardial damage with severe inflammation, and 4 = severe myocardial damage associated with multifocal necrotic tissue damage and severe inflammation [36].

Masson's Trichrome Staining

Myocardial tissues embedded in paraffin were sliced into sections with 5 µm thickness, stained by aniline Masson's trichrome blue stain. Sections were examined using optical microscopy with a magnification power 200× to determine the fraction size of interstitial and perivascular fibrosis.

Immunohistochemistry

Paraffin-embedded myocardial tissues were sectioned into 3 µm thickness using a microtome. Deparaffinization of myocardial tissues occurred, followed by antigen retrieval through a 20-minute heat treatment in boiling water (80 °C). Washing cycles, lasting five minutes between steps, were performed using 0.1 M phosphate buffer with pH 7.4. Cardiac tissue sections were treated with diluted rabbit polyclonal primary antibodies against α-SMA (1:200, ab5694, Abcam, Cambridge, UK) and Desmin (1:200, ab15200, Abcam, Cambridge, UK) for 16 hours, following the manufacturer's guidelines. The sections were visualized using a Leica DM2000 light microscope. Analysis of randomly selected fields (n = 6) per slide was conducted using image analysis software (Image-Pro Plus 5.0, Media Cybernetics, Rockville, MD, USA). Two independent pathologists blinded to the pathological findings performed histopathology and immunohistochemical staining, scoring, and quantification. The overall expressions of proteins were determined as the mean histoscore values.

Western Blotting

Cardiac tissue homogenates were boiled for five minutes, added to a loading buffer containing 2-mercaptoethanol, and applied to 12% sodium dodecyl sulfate-polyacrylamide gel electrophoresis (SDS-PAGE) gel. The gel ran for 2 hours at 100 volts. Subsequently, the proteins were transferred to polyvinylidene fluoride (PVDF) membranes and blocked using a tris-buffer blocking solution for 1 hour, containing 5% (w/v) non-fat milk and 0.05% Tween-20. The membranes were incubated overnight at 4 °C with primary antibodies: anti-Cleaved Caspase-3 (1:1000, ab214430, Abcam, Cambridge, UK), anti-heat shock protein 70 (anti-Hsp70, 1:1000, ab181606, Abcam, Cambridge, UK), and β-actin (1:1500, Santa Cruz Biotechnology, Santa Cruz, CA, USA). A goat anti-rabbit polyclonal immunoglobulin with horseradish peroxidase (1:5000) (Cell Signaling Technology Inc., Danvers, MA, USA) served as a secondary antibody. Bands were visualized using chemiluminescence, and protein bands were determined and quantified as fold change compared to the control group after normalization to β-actin protein using Image J (Fiji Imagej; 1.51 n, National Institute of Health , Bethesda, MD, USA) software.

Determination of Myocardial Tissue Total Protein

The protein content in the tissue homogenates was quantified using the Bradford technique, employing the Bio-Rad (#5000001, Hercules, CA, USA) protein assay kit.

Catalase Activity Determination in the Myocardial Tissue

This assay is employed to quantify the remaining levels of hydrogen peroxide in the cardiac tissue homogenate following the action of the catalase enzyme. Hydrogen peroxide was added to a known amount of catalase enzyme dissolved in a reaction buffer and incubated for 30 minutes at 28 °C. The enzymatic reaction was halted by adding sodium azide, and the produced color was assessed calorimetrically at 590 nm, using a commercial kit (ab83464, abcam, Waltham, MA, USA).

Lactate Dehydrogenase (LDH), Alanine Transaminase (ALT), and Aspartate Transaminase (AST) Determination

LDH, ALT, and AST are enzymes widely distributed in the body, with their highest levels found in the cardiac and hepatic tissues. The levels of these enzymes were significantly increased in case of myocardial injury. In the resent study, ALT, AST, and LDH enzyme activities were determined in rats sera using commercial assay kits (ab241035, ab105135 and ab102526 respectively, Abcam, Cambridge, UK).

Serum Creatine Kinase-MB (CK-MB) Determination

Creatine kinase (CK) activity in sera was determined calorimetrically by a commercial CK assay kit obtained from Abcam (ab285231, Cambridge, UK). The assay relies on reactions involving adenosine diphosphate and phosphocreatine, leading to the generation of an intermediate-colored product. The absorbance of this product can be determined at 450 nm.

Cardiac Troponin I Level Determination

Cardiac troponin I (CTNI) is a biomarker commonly used to indicate the extent of myocardial damage. Using an enzyme-linked immunosorbent assay (ELISA) technique, CTNI levels were determined in sera using the standard kit (# SEB820Ra, Fernhurst, TX 77494, O'ahu, HI, USA). The kit procedures depend on sandwich enzyme immunoassays to quantitatively determine CTNI in rats' serum.

Determination of SOD Activity

The enzyme activity of the superoxide dismutase (SOD) enzyme in cardiac tissue homogenate was determined using a standard commercial kit from Biodiagnos-

tics (# SD 2521, Cairo, Egypt). The methodology involves the addition of tetrazolium salts to the sample, producing formazan dye, whose increase in absorbance at 450 nm is measured.

Reduced Glutathione (GSH) Concentration Determination

The reduced glutathione (GSH) content in cardiac tissue homogenate was determined using a standard commercial kit from Biodiagnostics (GR 2511, Cairo, Egypt). The procedure followed the manufacturer's instructions and was based on reducing 5,5′-dithiobis-2-nitrobenzoic acid (DTNB) by tissue GSH, producing a yellow color, which was determined colorimetrically at 412 nm.

Glutathione Peroxidase (GSH-Px) Activity Determination

The activity of the glutathione peroxidase enzyme (GSH-Px) was determined in tissue homogenate using a standard biodiagnostics kit (GP 2524, Biodiagnostics, Cairo, Egypt). GSH-Px activity was determined at a wavelength of 412 nm, corresponding to the maximal absorbance of the enzyme-catalyzed reaction product.

Total Antioxidant Capacity Determination

A colorimetric assay based on the reaction between the antioxidants present in the sample and hydrogen peroxide (H_2O_2) determined total antioxidant capacity in rats. The amount of H_2O_2 that did not react with sample antioxidants was measured calorimetrically by converting it into a colored product, which can be determined at a wavelength of 510 nm.

Determination of Serum Lipid Levels in Rats

The lipid profiles of animals, including high-density lipoprotein (HDL # ab65390), total cholesterol (TC # ab65390), and triglyceride (TG # ab65336), were determined by using a commercial standard kit obtained from Abcam (Cambridge, UK) and following the manufacturer's instructions. Low-density lipoprotein (LDL) concentrations were determined using the equation LDL = TC – (HDL + VLDL), while very low-density lipoprotein (VLDL) = TG/5 (Abcam, Cambridge, UK).

Malondialdehyde (MDA) Content Determination

The assessment of the level of lipid peroxidation in the myocardial tissue was determined by estimating the levels of malondialdehyde (MDA) in tissue homogenates. This process is based on the reaction between thiobarbituric acid and MDA tissue content in an acidic medium at 95 °C, producing a pink color. The determination was performed at a wavelength of 532 nm [37,38].

Nitric Oxide (NO) Determination

Determining myocardial (NO) levels was conducted utilizing the Griess reaction, a colorimetric assay commonly used to determine NO levels. In this assay, Griess reagent (# ab234044) obtained from Abcam (Cambridge, UK) was added to the tissue sample homogenate, producing a deep purple color, which was measured spectrophotometrically at 540 nm [39,40].

Inflammatory Mediator's Level Determination

Serum levels of the inflammatory mediators interleukin-1 beta (IL-1β) and interleukin-6 (IL-6) were assessed using the enzyme-linked immunosorbent assay (ELISA) technique. The assessments followed the manufacturer's instructions by R&D Systems (Minneapolis, MN, USA).

Statistical Analysis

Statistical analysis in the present study was conducted using GraphPad Prism (version 9.2.0, Dotmatics, Boston, MA, USA). Values were displayed as the mean ± standard error of the mean (SEM). A one-way ANOVA test was employed to compare the obtained results, followed by the Tukey-Kramer test. The difference between groups was considered significant if $p < 0.05$.

Results

Characterization of CAP@CS Nanocapsules

As shown in Fig. 1, DLS measurements revealed an average particle size of 260 nm for the prepared CAP@CS nanocapsules, exhibiting a narrow PDI of 0.48. However, as presented in Fig. 2, TEM analysis depicted nanospheres with a diameter of approximately 220 nm. The zeta potentials of CS, CAP, and CAP@CS nanocapsules are measured to be +37.24 mV, –12.33 mV, and +21.23 mV, respectively. The encapsulation efficiency (EE) of CAP within the CAP@CS nanocapsules reached a maximum of 64.77 ± 1.26%.

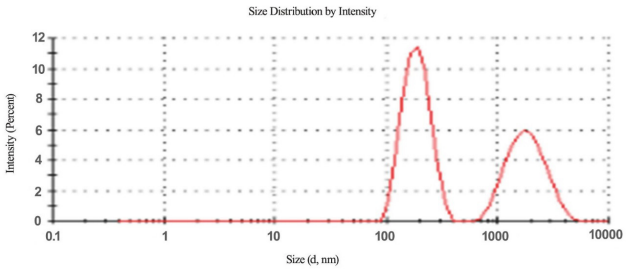

Fig. 1. Particle size distributions of capsaicin-loaded chitosan nanocapsules CAP@CS nanocapsules. CAP@CS, capsaicin-loaded chitosan nanocapsules.

Journal of
BIOLOGICAL REGULATORS
and Homeostatic Agents

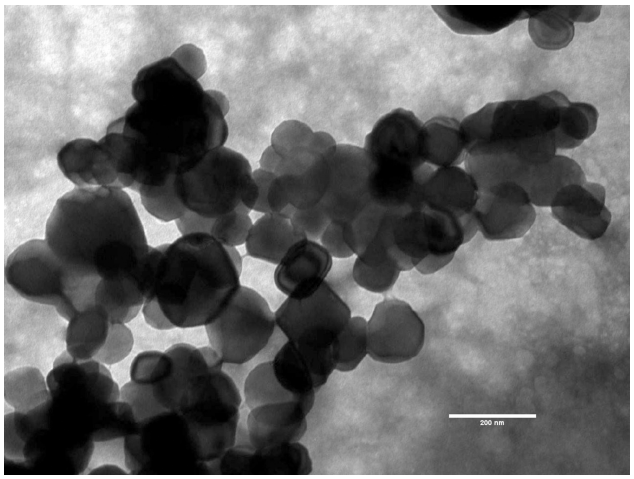

Fig. 2. TEM images of CAP@CS nanocapsules (scale bar represents 200 nm). TEM, transmission electron microscopy.

In Vitro Release of CAP from CAP@CS

Fig. 3 illustrates the dissolution profiles of CAP@CS nanocapsules and free CAP in phosphate buffer solution at pH 4 and 7.4. Within 10 hours, less than 3% of the free CAP in the dialysis bag was released, in contrast to 59.33% from the CAP@CS nanocapsules. Over the same period, the cumulative CAP release from CAP@CS nanocapsules was 51.15 % at pH 4 and 11.1% at pH 7.4 in the phosphate buffer.

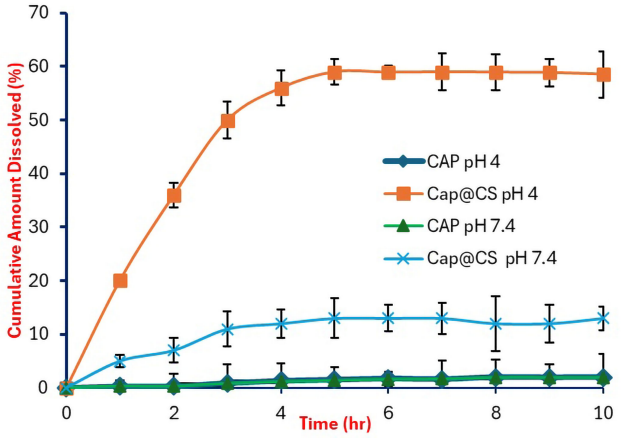

Fig. 3. Cumulative release of CAP@CS and free CAP under varying pH conditions. CAP, capsaicin.

Mathematical Modeling and Analysis of Release Kinetics

In vitro, release data from different parameters were analyzed using various kinetic models to understand the CAP release mechanism. Table 1 summarizes the regression coefficients (R^2) and release rate constants (k) for unmodified CAP and CAP@CS nanocapsules in phosphate buffers at pH 4 and 7.4. The Weibull model demonstrated the optimal fit for all cases, exhibiting significantly higher R^2 values for CAP@CS nanoparticles (0.9949 at pH 7.4 and 0.9987 at pH 4) compared to unmodified CAP (0.9737).

Stability Study

Stability studies were conducted at 4 °C and at room temperature for the CAP@CS nanocapsules, and the results are summarized in Table 2. It was found out that no considerable variations occurred. After 4 weeks of storage, the formulation showed a slight increase in size at 4 °C, and at room temperature, respectively, as 289.33 ± 7.19 and 338.66 ± 15.63, which were within the acceptable range. Further, the values of PDI were found to be 0.466 ± 0.02 and 0.554 ± 0.02. In addition, the zeta-potential values remained near –30 mV, which indicated the stability of the nanocapsules.

Table 1. Mathematical modeling and release kinetics of CAP and capsaicin-loaded chitosan nanocapsules (CAP@CS) nanocapsules at different pH conditions.

Kinetic Model		CAP@CS		CAP
		pH 4	pH 7.4	pH 7.4
Zero-Order	K_o	0.07	0.001	0.002
	R^2	0.97	0.9818	0.9135
First-Order	K_1	0.001	0	0
	R^2	0.9775	0.9842	0.9138
Higushi	kH	0.715	0.344	0.017
	R^2	0.9012	0.8622	0.9183
Korsmeyer-Peppas	kKP	0.18	0.6	0.006
	R^2	0.9972	0.9883	0.9732
Hixon-Crowell	kHC	0	0	0
	R^2	0.9751	0.9834	0.9137
Wiebull	β	0.742	0.731	0.571
	Ti	5.589	10.244	9.927
	R^2	0.9987	0.9949	0.9737

Table 2. Nanocapsule size, zeta potential, polydispersity index (PDI); entrapment efficiency (EE%) for the formulation stored at 4 °C and at room temperature for four weeks (n = 3).

Storage temperature	4 °C	Room temperature (25 °C)
Size (nm)	289.33 ± 7.19	338.66 ± 15.63
PDI	0.466 ± 0.02	0.554 ± 0.02
Zeta potential (mV)	+37.13 ± 0.92	+28.7 ± 0.57
EE%	57.63 ± 0.318	63.1 ± 1.7

Histopathological Results

H&E Staining

The control group (Fig. 4A) exhibited a normal myocardial tissue structure with regular myofiber striations. In contrast, the diabetic group (Fig. 4B) showed myocardial fiber separation, intense inflammatory cell infiltration, edema, and vacuolated cells with prominent inflammatory cell infiltration. The myocardial tissue appeared highly congested, and myocardial muscles were degenerated. Conversely, the rosuvastatin-treated group (Fig. 4C) demonstrated a moderate reduction in pathological changes in the myocardium. This included a moderate departure of myocardium striations, vacuolization of some myocardial cells, and upregulation of inflammatory cells relative to the normal control group. The CAP-treated group (Fig. 4D) exhibited a significant amelioration in the pathological changes in the myocardium, with a noticeable reduction in the inflammatory cell infiltration.

Moreover, the improvement was more pronounced in the CAP@CS-treated group (Fig. 4E) compared to the CAP-treated group. The damage score revealed (Fig. 4F) that damage level induced by DM was decreased when CAP@CS treatment was applied. The CAP@CS group showed no inflammatory cell infiltration and preserved normal cardiac fiber organization. The myocardial congestion was also significantly reduced, without any degeneration observed in the cardiac muscle.

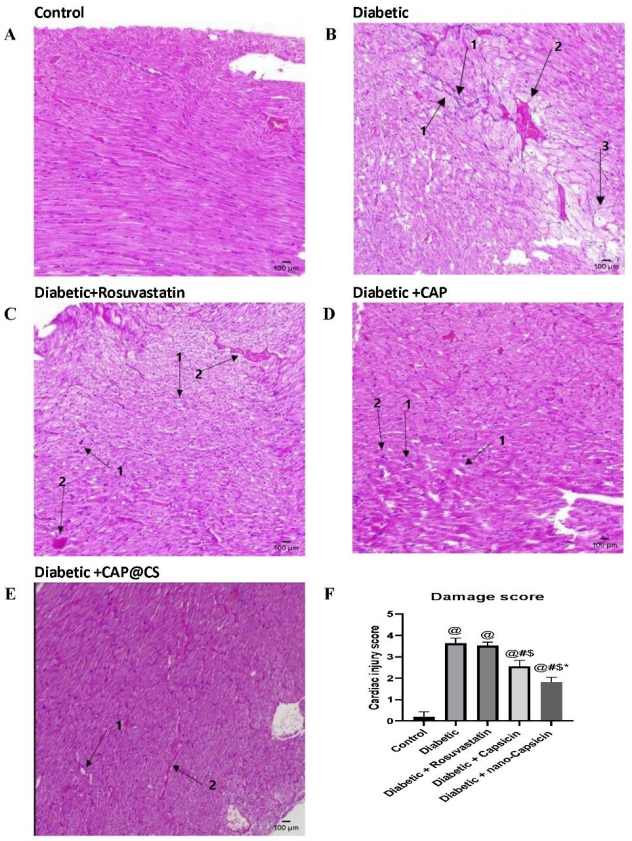

Fig. 4. Histopathology of rats' hearts (H&E stain, n = 6). (A) The control group, (B) the diabetic group, (C) the diabetic group received rosuvastatin, (D) the diabetic group received CAP, (E) the diabetic group received CAP@CS nanocapsules, and (F) damage score of cardiac muscle for all experimental groups. Arrows No 1 = inflammatory cells infiltration, No 2 = congestion and No 3 = vacuolization of some myocardial cells. @ = significantly different relative to the control group; # = significantly different relative to the diabetic group; $ = significantly different relative to the diabetic + rosuvastatin group; * = significantly different relative to the diabetic + CAP@CS group. H&E, hematoxylin and eosin.

Masson's Trichrome

The histopathological assessment of the cardiac muscle using Masson's trichrome revealed that the normal control group (Fig. 5A) had no collagenous fibers (×200). In contrast, the diabetic group (Fig. 5B) showed a significant increase in dense collagen deposition in the myocardial tissue, surrounding blood vessels, and fibrotic tissues found in the myocardium's interstitial and perivascular regions.

Rosuvastatin oral administration (Fig. 5C) moderately reduced collagen deposition and perivascular fibrosis. Moreover, the CAP-administered group (Fig. 5D) demonstrated a significant reduction in cardiac fibrosis and mild collagen deposition, while the CAP@CS nanocapsules-treated group (Fig. 5E) showed an intense reduction in the distribution of fibrotic tissue and collagen deposition. (Fig. 5F) showed that the diabetic group received CAP@CS nanocapsules has lowest fibrosis percentage.

Immunohistochemistry

Effects of CAP@CS Nanocapsules on α-SMA Protein Distribution

In diabetic rats (Fig. 6B), the levels of alpha-smooth muscle actin (α-SMA) protein immune expression in cardiac tissue were significantly higher than those noticed in the control group (Fig. 6A), which exhibited nearly no α-SMA protein expression. In contrast, the CAP-treated group (Fig. 6C) displayed weak staining of positive α-SMA distributed in different regions of the myocardium and around some perivascular areas, which was less noticeable than the rosuvastatin-treated group (Fig. 6D). Moreover, the CAP@CS nanocapsules-treated group (Fig. 6E,F) showed faint, lower immune expression of α-SMA compared to other treated diabetic groups.

Effects of CAP@CS Nanocapsules on Desmin Protein Distribution

The current study's immunohistopathological investigation of myocardial tissue revealed that the control group (Fig. 7A) exhibited strong positivity of desmin antibodies associated with normal stained Z-lines and intercalated disks. In diabetic rats (Fig. 7B), uneven faint stain-

Journal of
BIOLOGICAL REGULATORS
and Homeostatic Agents

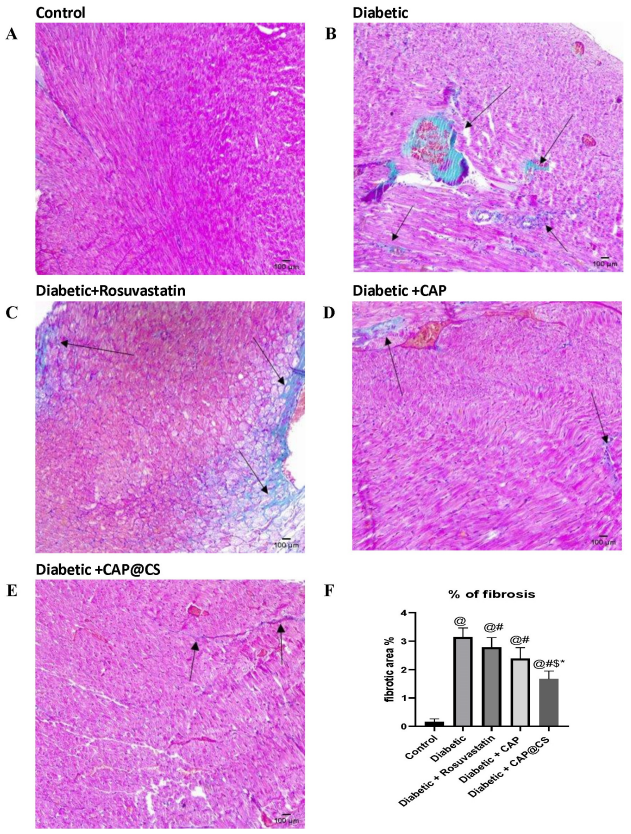

Fig. 5. Histopathology of rats' hearts (Masson trichrome stain, n = 6). (A) The control group, (B) the diabetic group, (C) the diabetic group received rosuvastatin, (D) the diabetic group received CAP, (E) the diabetic group received CAP@CS nanocapsules, and (F) fibrosis percentage of cardiac muscle for all experimental groups. Arrows pointed to myocardial fibrotic tissue. @ = significantly different relative to the control group; # = significantly different relative to the diabetic group; $ = significantly different relative to the diabetic + rosuvastatin group; * = significantly different relative to the diabetic + CAP@CS group.

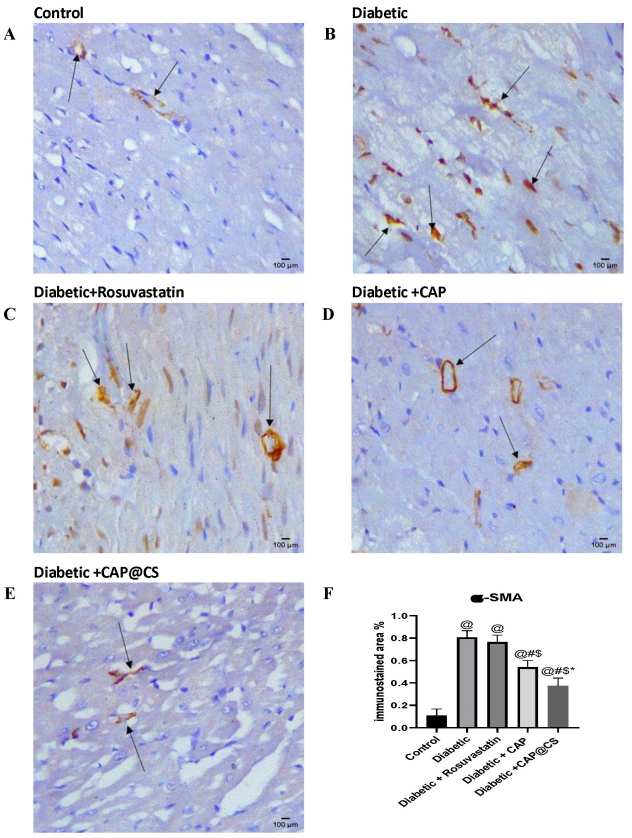

Fig. 6. Immunohistochemistry results of Alpha-Smooth Muscle Actin (α-SMA) in cardiac tissues (n = 6). (A) The control group, (B) the diabetic group, (C) the diabetic group received rosuvastatin, (D) the diabetic group received CAP, (E) the diabetic group received CAP@CS nanocapsules, and (F) distribution percentage of α-SMA for all experimental groups, wherease α-SMA was predominantly expressed in vascular medial smooth muscle cells, myocardial arterioles and in the border zone of damages myocardial tissue. Arrows pointed to α-SMA. @ = significantly different relative to the control group; # = significantly different relative to the diabetic group; $ = significantly different relative to the diabetic + rosuvastatin group; * = significantly different relative to the diabetic + CAP@CS group.

ing of desmin and cross-striation disarrangement were observed. Desmin staining was nearly normalized in the CAP-treated group (Fig. 7D), with some aggregation observed in the intermyofibrillar spaces. Meanwhile, the CAP@CS nanocapsules-treated group (Fig. 7E,F) showed consistent cross-striation patterns, intense staining at Z-lines, and intercalated disks, maintaining a consistent cross-striation pattern. Desmin staining was reduced in the rosuvastatin group (Fig. 7C), with considerable desmin alignment distortion.

Effects of CAP@CS on the Concentration of HO-1

In the present study, Western blotting was employed to examine the impact of oral administration of CAP@CS nanocapsules on the relative concentration of heme oxygenase-1 (HO-1) in rats' cardiac tissue (Fig. 8A,B). A comparison between the diabetic group and the CAP group revealed a significant increase in HO-1 relative concentration compared to the non-treated diabetic group. The oral administration of the CAP@CS nanocapsules produced a higher upregulatory effect on HO-1 relative concentration than all treated groups.

Effects of CAP@CS on the Relative Concentrations of HSP 70

The relative heat shock protein 70 (HSP70) amounts were determined using Western blot analysis. Compared to the control group, the diabetic group showed nearly a five-fold upregulation in the relative concentration of HSP70. Rosuvastatin oral treatment led to a moderate decrease in HSP70 concentration, albeit significantly less than the re-

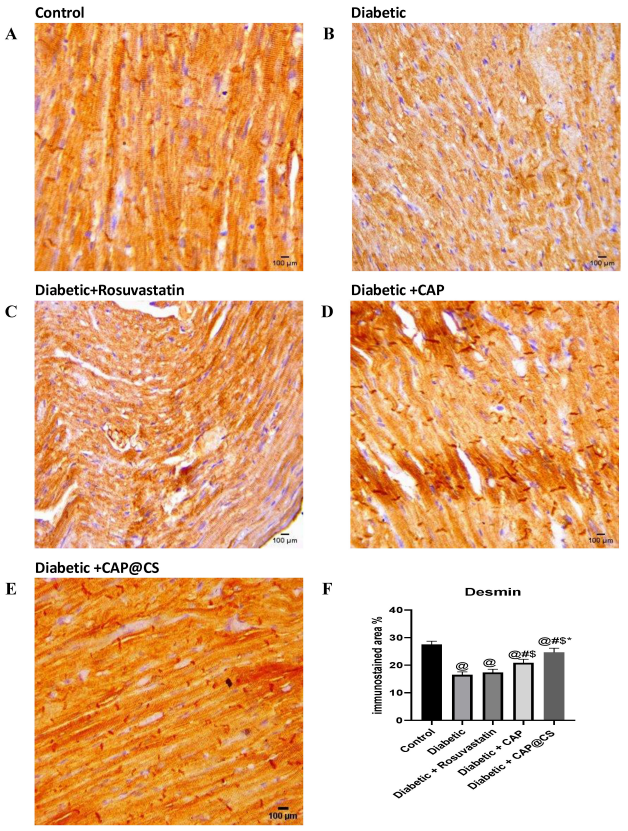

Fig. 7. Immunohistochemistry results of desmin in cardiac tissues (n = 6). (A) The control group, (B) the diabetic group, (C) the diabetic group received rosuvastatin, (D) the diabetic group received CAP, (E) diabetic group received CAP@CS nanocapsules, and (F) distribution percentage of desmin for all experimental groups, wherease Desmin was found at myocardial Z-discs and link myofibrils to one another, to the sarcolemma, and to the myocardial nuclear envelope, @ = significantly different relative to the control group; # = significantly different relative to the diabetic group; $ = significantly different relative to the diabetic + rosuvastatin group; * = significantly different relative to the diabetic + CAP@CS group.

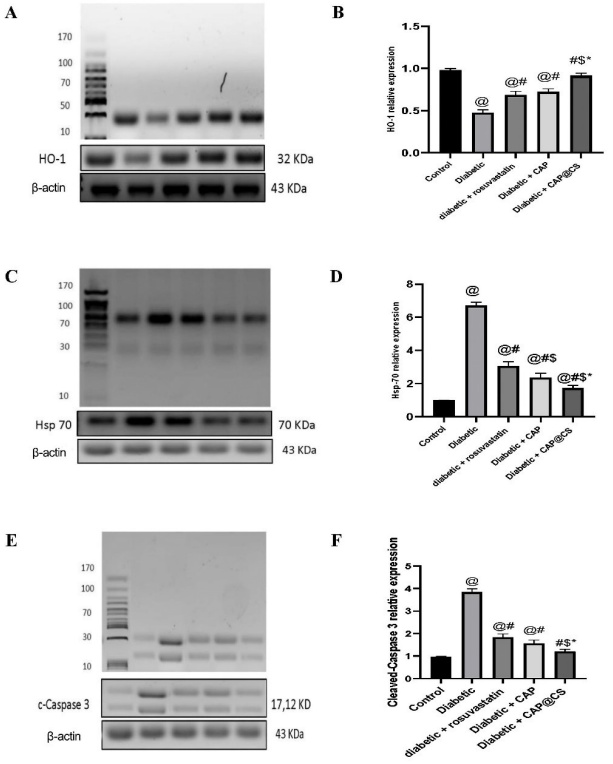

Fig. 8. Effect of CAP@CS administration on HO-1, HSP 70 and cleaved caspase-3 myocardial protein expression. Hence, (A) and (B) figures refer to HO-1 myocardial protein expression, (C) and (D) figures refer to Heat shock protein 70 (HSP 70) myocardial protein expression, (E) and (F) figures refer to cleaved caspase-3 myocardial protein expression. The quantitative analysis was represented as a relative expression, and protein expression was normalized against beta-actin, @ = significantly different relative to the control group; # = significantly different relative to the diabetic group; $ = significantly different relative to the diabetic + rosuvastatin group; * = significantly different relative to the diabetic + CAP@CS group. Results were displayed as mean ± standard error of the mean (SEM) (n = 3). HO-1, heme oxygenase-1.

duction achieved with CAP. Notably, the CAP@CS-treated group displayed the lowest concentration of HSP70 among all treated diabetic groups, as depicted in Fig. 8C,D.

Effects of CAP on Cleaved Caspase-3 Relative Concentration

Western blotting analysis was employed to assess the relative amounts of cleaved caspase-3 in rats' cardiac tissue (Fig. 8E,F) to evaluate the effectiveness of CAP@CS nanocapsules as an anti-apoptotic agent. The results indicated a significantly ($p < 0.05$) higher relative concentration of cleaved caspase-3 in the diabetic group compared to the control group. Rosuvastatin oral administration weakly attenuated cleaved caspase-3 upregulation. Conversely, CAP administration significantly ($p < 0.05$) attenuated cleaved caspase-3 upregulation, although this attenuating effect was significantly lower than observed in the CAP@CS nanocapsules-treated group.

Effect of CAP on Lipid Profile

Serum triglyceride (Fig. 9A), low-density lipoprotein (Fig. 9B), very low-density lipoprotein (Fig. 9C), and TC levels (Fig. 9D) in diabetic rats fed on HFD were significantly increased, surpassing levels observed in the control group. Furthermore, compared to the control group, diabetic rats fed on HFD exhibited a significant decrease in HDL levels, as illustrated in Fig. 9E. Treating diabetic rats with CAP@CS nanocapsules led to a significant decrease in TG, TC, LDL, and VLDL levels, which were lower than in the CAP-treated group but not significantly different from the rosuvastatin-treated group. Moreover, compared to the

Journal of
BIOLOGICAL REGULATORS
and Homeostatic Agents

diabetic HFD group, CAP@CS nanocapsules treatment significantly increased HDL levels, which were higher than the CAP-treated group but not significantly higher than the rosuvastatin-treated group.

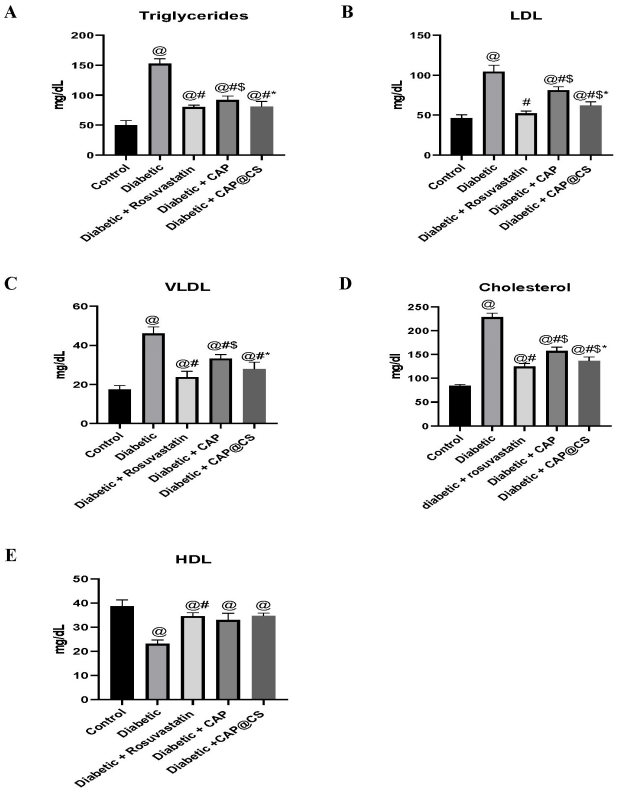

Fig. 9. Effect of CAP@CS administration on the levels of serum lipids. (A) Triglyceride (TG), (B) low-density lipoprotein (LDL), (C) very low-density lipoprotein (VLDL), (D) total cholesterol (TC), and (E) high-density lipoprotein (HDL). @ = significantly different relative to the control group, # = significantly different relative to the diabetic group, $ = significantly different relative to the diabetic + rosuvastatin group, * = significantly different relative to the diabetic + CAP@CS group. Results were displayed as mean ± SEM (n = 12).

Effect on Oxidative Stress Parameters

As depicted in Fig. 10A, the antioxidant enzymes SOD, catalase (Fig. 10B), and glutathione peroxidase (GSH-Px) (Fig. 10C) were significantly lower in diabetic rats fed on HFD compared to the control group, which exhibited higher concentrations. Oral administration of CAP@CS nanocapsules significantly ameliorated the depletion of these enzymes, and these ameliorative effects were significantly more potent than the effects observed with CAP alone.

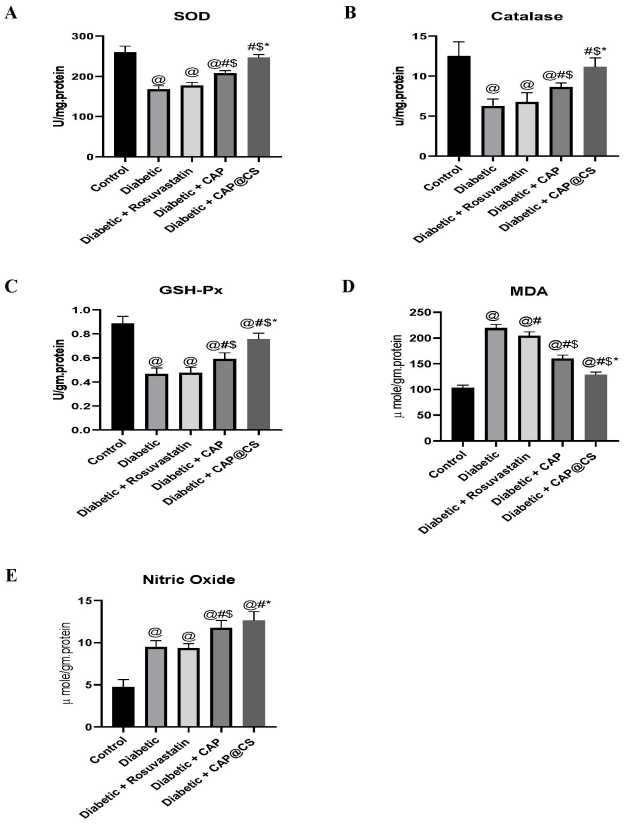

Fig. 10. Effect of CAP@CS administration on oxidative stress parameters. (A) Superoxide dismutase (SOD), (B) catalase, (C) glutathione peroxidase (GSH-Px), (D) malondialdehyde (MDA), and (E) nitric oxide. @ = significantly different relative to the control group, # = significantly different relative to the diabetic group, $ = significantly different relative to the diabetic + rosuvastatin group, * = significantly different relative to the diabetic + CAP@CS group. Results were displayed as mean ± SEM (n = 12).

Effect of CAP@CS Administration on Lipid Peroxidation

The malondialdehyde (MDA) level (Fig. 10D), a commonly used biomarker for evaluating tissue lipid peroxidation, was examined in this study. Oral treatment by CAP significantly protected rats' myocardium against lipid peroxidation, and the MDA concentration in the myocardial was significantly lower than the determined concentrations observed in the untreated diabetic and rosuvastatin-treated groups. Moreover, the CAP@CS nanocapsules-treated group exhibited the lowest observed MDA concentrations among all treated groups.

Effect of CAP on NO Level

As shown in Fig. 10E, the diabetic group exhibited a noticeable upregulation in the myocardial tissue content of nitric oxide (NO) compared to the control group, which was further increased by oral administration of CAP. However, the highest nitric oxide concentration was observed in the

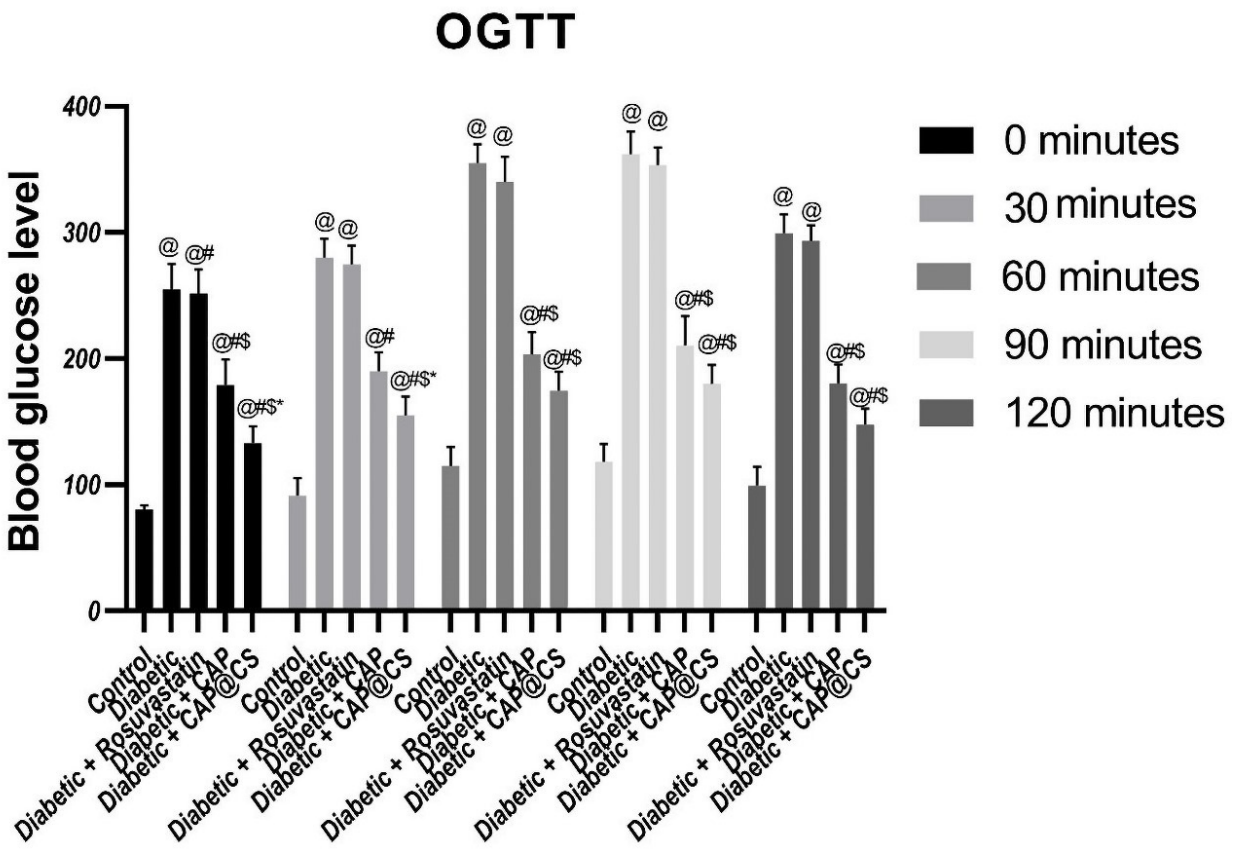

Fig. 11. Effect of CAP@CS administration on blood glucose levels at 0, 30, 60, 90, and 120 min of oral glucose tolerance test (OGTT). @ = significantly different relative to the control group, # = significantly different relative to the diabetic group, $ = significantly different relative to the diabetic + rosuvastatin group, * = significantly different relative to the diabetic + CAP@CS group. Results were displayed as mean ± SEM (n = 12).

CAP@CS nanocapsules-treated group, while the oral administration of rosuvastatin did not affect nitric oxide concentrations in cardiac tissue.

Comparison of Blood Glucose Levels in Rats

During the OGTT, rats orally administered CAP exhibited substantially lower blood glucose levels at 0 minutes, 30 minutes, 60 minutes, 90 minutes, and 120 minutes compared to the diabetic non-treated group. In contrast, the group treated with CAP@CS nanocapsules exhibited the most substantially reduced OGTT values compared to the other diabetic groups (Fig. 11). Oral administration of rosuvastatin did not affect a statistically significant change in blood glucose levels.

Effect of CAP@CS on Inflammatory Mediators

The elevated levels of interleukin-6 (IL-6), interleukin-1 beta (IL-1β) and tumor necrosis factor-alpha (TNF-α) in diabetic animals that were administered a high-fat diet (HFD) were evident in Fig. 12A–C respectively, in comparison to the control group. In contrast, the administration of CAP via oral route resulted in a substantial reduction ($p < 0.05$) in the IL-6 and IL-1β concentrations compared to the diabetic and rosuvastatin-treated groups. Notably, the lowest concentration of both inflammatory mediators was observed in the CAP@CS nanocapsules-treated group.

Effect of CAP@CS on Cardiac Enzymes

In this work, the diabetic rats exhibited significantly higher levels of the cardiac enzymes CK (Fig. 12D), lactate dehydrogenase (LDH) (Fig. 12E), and cardiac troponin I (CTNI) (Fig. 12F) than those observed in the control group. Oral treatment with CAP significantly reduced the levels of these enzymes compared to the diabetic group. In contrast, CAP@CS oral administration significantly ameliorated these enzymes, whereas rosuvastatin administration produced a moderately reducing effect.

The activities of AST (Fig. 13B) and ALT (Fig. 13A) in cardiac tissue were significantly reduced after oral administration of CAP in comparison to the diabetic group. However, the CAP@CS-treated group exhibited substantially lower values in these parameters than the CAP-treated group. On the other hand, the rosuvastatin-treated group also showed a significant decrease in both ALT and AST tissue activities.

Journal of
BIOLOGICAL REGULATORS
and Homeostatic Agents

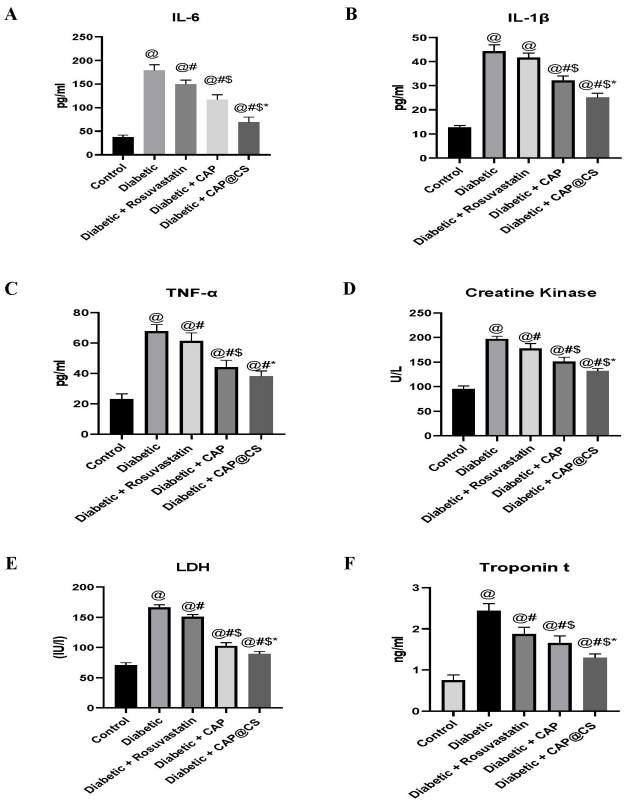

Fig. 12. Effect of CAP@CS administration on the inflammatory and cardiac enzymes parameters. (A) Interleukin-6 (IL-6), (B) Interleukin-1 beta (IL-1β), (C) Tumor necrosis factor-alpha (TNF-α), (D) Creatine kinase (CK), (E) Lactate dehydrogenase (LDH), and (F) Cardiac troponin I in the normal and treated animals. @ = significantly different relative to the control group, # = significantly different relative to the diabetic group, $ = significantly different relative to the diabetic + rosuvastatin group, * = significantly different relative to the diabetic + CAP@CS group. Results were displayed as mean ± SEM (n = 12).

Discussion

Chitosan (CS), derived from partially deacetylated chitin with a positive charge, is a promising drug carrier. Chitosan nanoparticles enhance poorly soluble drugs' solubility and oral absorption. Capsaicin (CAP), the pungent alkaloid in chili peppers, possesses various therapeutic benefits, including antioxidant activity. As a negatively charged molecule, CAP readily forms stable complexes with chitosan through electrostatic interactions, facilitating sustained drug release.

This study explored using a chitosan-based system to develop a nanocarrier loaded with hydrophobic CAP. The objective was to evaluate the efficacy of this system in ameliorating cardiac myopathy in a rat model of T2DM.

The CAP@CS nanocapsules were formulated using a microemulsion technique. TEM revealed the formation of uniform, circular nanospheres with a diameter of approximately 220 nm. However, DLS measurements indicated an average size of approximately 260 nm. This difference is probably due to the solvent effect causing the hydrated nanocapsules to swell in solution, leading to a larger size when measured by DLS.

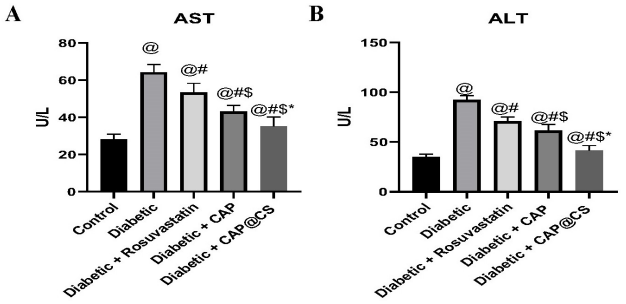

Fig. 13. Effect of CAP@CS on the levels of (A) AST and (B) ALT in the normal and treated rats. @ = significantly different relative to the control group, # = significantly different relative to the diabetic group, $ = significantly different relative to the diabetic + rosuvastatin group, * = significantly different relative to the diabetic + CAP@CS group. Results were displayed as mean ± SEM (n = 12). AST, aspartate transaminase; ALT, alanine transaminase.

Zeta potential measurements showed negative potential for CAP and positive potential for CAP@CS, indicating the successful encapsulation of the negatively charged CAP molecules within the positively charged chitosan matrix.

The release profile of CAP@CS nanocapsules exhibited pH dependence. A rapid burst release was observed at pH 4 (59.33% in 4 hours), which was significantly ($p < 0.001$) lower than that observed at pH 7.4 (11.1% in 4 hours). The cumulative release of CAP plateaued at both pH values after 4 hours, with no significant difference ($p > 0.05$).

The hypothesis suggests that the controlled release mechanism of CAP@CS nanocapsules is related to pH-induced structural changes in the capsules. Wang W *et al*. (2018) [41] demonstrated that CAP@CS nanocapsules swell considerably under acidic conditions (e.g., pH 4) due to the protonation of amino groups within the polymer shell. This swelling likely opens up pores or weakens the capsule structure, thereby facilitating the diffusion and release of encapsulated CAP.

Type 2 diabetics have a two- to fourfold increased risk of developing cardiovascular morbidities compared to those without the disease, according to the American Heart Association [42,43]. Despite an abundance of research in this field, there is no pharmaceutical treatment that explicitly targets the various types of cardiac damage that people with T2DM may experience.

The present study aims to explore the therapeutic potential of CAP@CS nanocapsules in mitigating myocardial damage induced by type 2 diabetes mellitus (T2DM).

A T2DM-induced myocardial damage model was established in animals, exhibiting disrupted myocardial integrity, widened interstitial spaces, focal necrosis of muscle fibers, and inflammatory cell infiltration. These results align with findings from previous reports [44,45].

The oral administration of CAP demonstrated promising results, decreasing the extent of diffused necrosis, reducing inflammatory cell infiltration, and mitigating myocardial damage. CAP's observed efficacy was superior to that of rosuvastatin, a commonly used reference drug.

The most significant protective effect against T2DM-induced myocardial injury was observed in animals treated with CAP@CS nanocapsules. This formulation demonstrated a remarkable reduction in the histological score of cardiac injury, surpassing all other treatment groups.

Desmin, as a critical intermediate filament protein for the construction and function of cardiomyocytes, plays a crucial role in maintaining the myocardium's integrity and serving as a platform for intracellular signaling. Disruption of desmin can result in cardiomyopathy [46,47]. In this study, CAP and CAP@CS oral administration were found to significantly maintain desmin's normal integrity in the myocardial tissue of diabetic rats. This effect was more prominent in the CAP@CS-treated group than in the CAP-treated group.

In normal cardiac tissue, quiescent fibroblast-like cells are abundant. Nevertheless, in myocardial injurious activities, these cells transform into activated α-SMA-positive myofibroblasts [48,49]. Myofibroblasts release extracellular matrix proteins to protect heart muscle against rupture [50]. However, the overproduction of activated fibroblasts might contribute to the development of cardiac fibrosis, leading to increased rigidity and impaired systolic and diastolic functions [51,52]. Consistent with previous studies, the current investigation observed a substantial increase in both α-SMA and myocardial fibrosis in the diabetic animal model. However, CAP@CS administration significantly ameliorated these pathological changes more than the CAP-treated and standard drug (rosuvastatin)-treated groups. This amelioration may be mediated via activating TRPV1 receptors, inhibiting the TGF-β1/Smad2/3 signaling pathway, and ameliorating cardiac myofibroblast activation.

Cardiac remodeling in cases of extensive myocardial injury is frequently initiated by alterations in the extracellular matrix, fibrosis, and apoptosis [53]. These processes frequently result from oxidative stress and excessive oxidation of fatty acid [54]. Additionally, diabetes can induce cardiomyopathy via different pathways, including glucose transition metal-catalyzed autoxidation, leading to the production of hydrogen peroxide (H_2O_2), superoxide anion (O2-), and reactive dicarbonyl metabolites [55,56]. Consistent with these mechanisms, our study observed significant myocardial damage in diabetic rats with an intense upregulation of MDA cardiac tissue concentrations, accompanied by a remarkable reduction of the antioxidant enzymes catalase, SOD, and glutathione peroxidase.

Studies have provided evidence supporting the potent antioxidant capabilities of CAP, ameliorating intracellular oxidative stress [42,57,58]. CAP's antioxidant effects can be mediated by influencing the cellular expression of heat shock protein 1, increasing the expression of the mRNA of hydroperoxide glutathione peroxidase and SOD, resulting in amelioration of elevated levels of the cellular MDA and protection against reduced glutathione and catalase enzyme depletion caused by oxidative stress [23,59]. The present study observed that CAP oral administration significantly ameliorated SOD, glutathione peroxidase (GPx), catalase, and myocardial GSH tissue depletion. Furthermore, the CAP@CS oral administration nearly normalized these antioxidant cardiac tissue concentrations.

Heme oxygenase (HO) is a cellular component that is critical in protecting against oxidative stress. It exists in two forms: HO-1 (inducible) and HO-2 (constitutive). The inducible form (HO-1) can induce heme degradation, producing carbon monoxide (CO), iron, and biliverdin, which are further converted into bilirubin [60,61]. Both bilirubin and biliverdin are potent antioxidants, capable of increasing the tissue levels of the antioxidant enzymes SOD, catalase, and GPx [62]. The study observed that cap oral administration significantly upregulated HO-1 myocardial expression, and the CAP@CS formula significantly enhanced this effect.

Studies on CAP have confirmed its ability to reduce daily calorie consumption, enhance the release of glucagon-like peptide-1 (GLP-1), and decrease the small intestine's absorption of glucose. These effects are primarily mediated via the activation of TRPV1 receptors [63–65]. Moreover, CAP administration has been reported to upregulate muscular insulin receptor expression and reduce plasma leptin levels [66]. Additionally, the CAP can enhance lipid metabolism, promote lipolysis, and stimulate hepatocytes' lipid autophagy [67]. The study aligns with these findings, showing that CAP significantly reduced blood glucose levels and improved diabetic rats' lipid profiles. Interestingly, the newly formulated CAP@CS showed even higher hypoglycemic and hypolipidemic effects than CAP alone.

Apoptosis is a significant pathological feature in myocardial injury, and it can lead to necrosis and determinantal cardiac damage [68]. Caspase-3 is an initiator and executioner protein of cellular apoptosis, significantly upregulated in the case of cardiomyopathy, precisely its active form, cleaved caspase-3 [69]. The Western blot technique was utilized to assess the impact of CAP@CS on myocardial apoptosis. The results demonstrated that CAP@CS significantly decreased myocardial apoptosis by decreasing the upregulated concentrations of cleaved caspase-3. This effect was more potent than in the CAP and rosuvastatin-treated groups.

Chronic inflammation, as found in the case of diabetes, is a crucial factor in developing cardiomyopathy

Journal of
BIOLOGICAL REGULATORS
and Homeostatic Agents

[70]. Hyperglycemia can enhance the release of different types of cytokines through the activation of receptors for damage-associated molecular patterns (DAMP) and pathogen-associated molecular patterns. The NLR family pyrin domain-containing 3 (NLRP3) inflammatory pathway can mimic the effects of inflammatory cytokines, including NF-κB, TNF-α, IL-6, IL-1β, and IL-18, leading to leukocyte infiltration into the myocardium [71,72]. These released cytokines can activate cardiac fibroblasts, causing interstitial cardiac fibrosis formation [73]. The findings of this study align with these mechanisms. However, researchers suggested that CAP exhibited an anti-inflammatory effect by activating PPARγ receptors and promoting the expression of liver X receptor alpha (LXRα), inhibiting the release of inflammatory cytokines [74]. In agreement with these findings, the present study demonstrated a remarkable reduction in the inflammatory cytokines and leucocyte infiltration after oral administration of CAP@CS, indicating a higher anti-inflammatory effect than CAP.

HSP70 upregulation has been noticed in patients with cardiomyopathy, and increased levels of HSP70 are positively correlated with the development of myocardial dysfunction and remodeling. It has been reported that HSP70 inhibition can improve myocardial dysfunction. The Western blotting procedure [75] employed in this study showed that CAP oral administration decreased HSP 70 levels in diabetic rats, and this effect was significantly enhanced by using our new formula, CAP@CS.

The intracellular calcium influx, facilitated by connexin 43, is enhanced by the activation of TRPV1 receptors, which can be activated by CAP administration, increasing the expression of molecules involved in lipid metabolism [76]. Additionally, it has been observed that CAP can augment the expression of TRPV1 receptors, which are downregulated by an HFD, activating the AMP-activated protein kinase pathway and leading to an increase in glucose and fatty acid levels [66,76]. Consistent with these results, a significant decrease was observed in the levels of triglycerides, LDL, VLDL, and cholesterol in the group treated with CAP compared to the diabetic group. This effect was significantly enhanced by using the CAP@CS form, which produced an intense hypoglycemic effect in diabetic rats compared to CAP alone.

Conclusion

The present study introduced a new CAP@CS formulation of CAP offering a distinctive pharmacological property that was more potent than the parent compound CAP in ameliorating cardiac injury in diabetic rats.

Availability of Data and Materials

All data generated or analyzed during this study are included in this published article. The datasets used and/or analyzed during the present study are available from the corresponding author on reasonable request.

Author Contributions

RA designed and performed the research study, analyzed the data and wrote the manuscript. RA read and approved the final manuscript. RA have participated sufficiently in the work and agreed to be accountable for all aspects of the work.

Ethics Approval and Consent to Participate

All animal experiments were ratified according to the guidelines of the Standing Committee of Bioethics Research (Approval No. 222/2024) at Prince Sattam Bin Abdulaziz University.

Acknowledgment

I would like to show my appreciation to Dr. Adel M. Ahmed and Dr. Esam M. Aboubakr for their support and assistance in study design and carrying out the experiments.

Funding

This research received no external funding.

Conflict of Interest

The author declares no conflict of interest.

References

[1] Cho NH, Shaw JE, Karuranga S, Huang Y, da Rocha Fernandes JD, Ohlrogge AW, *et al*. IDF Diabetes Atlas: Global estimates of diabetes prevalence for 2017 and projections for 2045. Diabetes Research and Clinical Practice. 2018; 138: 271–281.

[2] Abdel-Moneim A, El-Shahawy A, Yousef AI, Abd El-Twab SM, Elden ZE, Taha M. Novel polydatin-loaded chitosan nanoparticles for safe and efficient type 2 diabetes therapy: *In silico*, *in vitro* and *in vivo* approaches. International Journal of Biological Macromolecules. 2020; 154: 1496–1504.

[3] Charlton A, Garzarella J, Jandeleit-Dahm KAM, Jha JC. Oxidative Stress and Inflammation in Renal and Cardiovascular Complications of Diabetes. Biology. 2020; 10: 18.

[4] De Geest B, Mishra M. Role of Oxidative Stress in Diabetic Cardiomyopathy. Antioxidants (Basel, Switzerland). 2022; 11: 784.

[5] Chien CY, Wen TJ, Cheng YH, Tsai YT, Chiang CY, Chien CT. Diabetes Upregulates Oxidative Stress and Downregulates Cardiac Protection to Exacerbate Myocardial Ischemia/Reperfusion Injury in Rats. Antioxidants (Basel, Switzerland). 2020; 9: 679.

[6] Frati G, Schirone L, Chimenti I, Yee D, Biondi-Zoccai G, Volpe M, *et al*. An overview of the inflammatory signalling mechanisms in the myocardium underlying the development of diabetic cardiomyopathy. Cardiovascular Research. 2017; 113: 378–388.

[7] Lu Q, Zheng R, Zhu P, Bian J, Liu Z, Du J. Hinokinin alleviates high fat diet/streptozotocin-induced cardiac injury in mice through modulation in oxidative stress, inflammation and apoptosis. Biomedicine & Pharmacotherapy. 2021; 137: 111361.

[8] Jafernik K, Ładniak A, Blicharska E, Czarnek K, Ekiert H, Wiącek AE, *et al*. Chitosan-Based Nanoparticles as Effective Drug Delivery Systems-A review. Molecules (Basel, Switzerland). 2023; 28: 1963.
[9] Rudramurthy GR, Swamy MK, Sinniah UR, Ghasemzadeh A. Nanoparticles: Alternatives Against Drug-Resistant Pathogenic Microbes. Molecules (Basel, Switzerland). 2016; 21: 836.
[10] Mohammed MA, Syeda JTM, Wasan KM, Wasan EK. An Overview of Chitosan Nanoparticles and Its Application in Non-Parenteral Drug Delivery. Pharmaceutics. 2017; 9: 53.
[11] Alshawwa SZ, Kassem AA, Farid RM, Mostafa SK, Labib GS. Nanocarrier Drug Delivery Systems: Characterization, Limitations, Future Perspectives and Implementation of Artificial Intelligence. Pharmaceutics. 2022; 14: 883.
[12] Herdiana Y, Wathoni N, Shamsuddin S, Muchtaridi M. Drug release study of the chitosan-based nanoparticles. Heliyon. 2021; 8: e08674.
[13] Arora V, Campbell JN, Chung MK. Fight fire with fire: Neurobiology of capsaicin-induced analgesia for chronic pain. Pharmacology & Therapeutics. 2021; 220: 107743.
[14] Mikulska P, Malinowska M, Ignacyk M, Szustowski P, Nowak J, Pesta K, *et al*. Ashwagandha *(Withania somnifera)*-Current Research on the Health-Promoting Activities: A Narrative Review. Pharmaceutics. 2023; 15: 1057.
[15] Merritt JC, Richbart SD, Moles EG, Cox AJ, Brown KC, Miles SL, *et al*. Anti-cancer activity of sustained release capsaicin formulations. Pharmacology & Therapeutics. 2022; 238: 108177.
[16] Periferakis AT, Periferakis A, Periferakis K, Caruntu A, Badarau IA, Savulescu-Fiedler I, *et al*. Antimicrobial Properties of Capsaicin: Available Data and Future Research Perspectives. Nutrients. 2023; 15: 4097.
[17] Hamed M, Kalita D, Bartolo ME, Jayanty SS. Capsaicinoids, Polyphenols and Antioxidant Activities of *Capsicum annuum*: Comparative Study of the Effect of Ripening Stage and Cooking Methods. Antioxidants (Basel, Switzerland). 2019; 8: 364.
[18] Dhamodharan K, Sankaran M. Chemomodulatory Effect of Capsaicin Encapsulated Chitosan Nanoparticles on Lipids, Lipoproteins and Glycoprotein Components in 7,12-Dimethylbenz[a]anthracene (DMBA) Induced Mammary Carcinogenesis in Sprague-Dawley Rats. Eurasian Journal of Medicine and Oncology. 2021; 5: 350–357.
[19] Ahmady AR, Solouk A, Saber-Samandari S, Akbari S, Ghanbari H, Brycki BE. Capsaicin-loaded alginate nanoparticles embedded polycaprolactone-chitosan nanofibers as a controlled drug delivery nanoplatform for anticancer activity. Journal of Colloid and Interface Science. 2023; 638: 616–628.
[20] Wu X, Xu N, Cheng C, McClements DJ, Chen X, Zou L, *et al*. Encapsulation of hydrophobic capsaicin within the aqueous phase of water-in-oil high internal phase emulsions: Controlled release, reduced irritation, and enhanced bioaccessibility. Food Hydrocolloids. 2022; 123: 107184.
[21] Han J, Zhang S, Liu X, Xiao C. Fabrication of capsaicin emulsions: improving the stability of the system and relieving the irritation to the gastrointestinal tract of rats. Journal of the Science of Food and Agriculture. 2020; 100: 129–138.
[22] Yi TF, Chang H, Wei TT, Qi SY, Li Y, Zhu YR. Approaching high-performance electrode materials of ZnCo2S4 nanoparticle wrapped carbon nanotubes for supercapacitors. Journal of Materiomics. 2021; 7: 563–576.
[23] Zhu Y, Peng W, Zhang J, Wang M, Firempong CK, Feng C, *et al*. Enhanced oral bioavailability of capsaicin in mixed polymeric micelles: Preparation, *in vitro* and *in vivo* evaluation. Journal of Functional Foods. 2014; 8: 358–366.
[24] Giri TK, Bhowmick S, Maity S. Entrapment of capsaicin loaded nanoliposome in pH responsive hydrogel beads for colonic delivery. Journal of Drug Delivery Science and Technology. 2017; 39: 417–422.
[25] Zhao Q, Wang J, Yin C, Zhang P, Zhang J, Shi M, *et al*. Near-Infrared Light-Sensitive Nano Neuro-Immune Blocker Capsule Relieves Pain and Enhances the Innate Immune Response for Necrotizing Infection. Nano Letters. 2019; 19: 5904–5914.
[26] Lu M, Cao Y, Ho CT, Huang Q. The enhanced anti-obesity effect and reduced gastric mucosa irritation of capsaicin-loaded nanoemulsions. Food & Function. 2017; 8: 1803–1809.
[27] Chatzēiōannou TP. Quantitative Calculations in Pharmaceutical Practice and Research. VCH. 1993.
[28] Li Y, Meng Q, Yang M, Liu D, Hou X, Tang L, *et al*. Current trends in drug metabolism and pharmacokinetics. Acta Pharmaceutica Sinica. B. 2019; 9: 1113–1144.
[29] HIGUCHI T. MECHANISM OF SUSTAINED-ACTION MEDICATION. THEORETICAL ANALYSIS OF RATE OF RELEASE OF SOLID DRUGS DISPERSED IN SOLID MATRICES. Journal of Pharmaceutical Sciences. 1963; 52: 1145–1149.
[30] Korsmeyer RW, Gurny R, Doelker E, Buri P, Peppas NA. Mechanisms of solute release from porous hydrophilic polymers. International Journal of Pharmaceutics. 1983; 15: 25–35.
[31] Hixson A, Crowell J. Dependence of reaction velocity upon surface and agitation. Industrial & Engineering Chemistry. 1931; 23: 923–931.
[32] Alexopoulos A. One-Parameter Weibull-Type Distribution, Its Relative Entropy with Respect to Weibull and a Fractional Two-Parameter Exponential Distribution. Stats. 2019; 2: 34–54.
[33] Barrière DA, Noll C, Roussy G, Lizotte F, Kessai A, Kirby K, *et al*. Combination of high-fat/high-fructose diet and low-dose streptozotocin to model long-term type-2 diabetes complications. Scientific Reports. 2018; 8: 424.
[34] Kim DH, Choi BH, Ku SK, Park JH, Oh E, Kwak MK. Beneficial Effects of Sarpogrelate and Rosuvastatin in High Fat Diet/Streptozotocin-Induced Nephropathy in Mice. PloS One. 2016; 11: e0153965.
[35] Szallasi A. Dietary Capsaicin: A Spicy Way to Improve Cardio-Metabolic Health? Biomolecules. 2022; 12: 1783.
[36] Qin-Wei Z, Yong-Guang LI. Berberine attenuates myocardial ischemia reperfusion injury by suppressing the activation of PI3K/AKT signaling. Experimental and Therapeutic Medicine. 2016; 11: 978–984.
[37] Placer ZA, Cushman LL, Johnson BC. Estimation of product of lipid peroxidation (malonyl dialdehyde) in biochemical systems. Analytical Biochemistry. 1966; 16: 359–364.
[38] Aboubakr EM, Taye A, Aly OM, Gamal-Eldeen AM, El-Moselhy MA. Enhanced anticancer effect of Combretastatin A-4 phosphate when combined with vincristine in the treatment of hepatocellular carcinoma. Biomedicine & Pharmacotherapy. 2017; 89: 36–46.
[39] Bryan NS, Grisham MB. Methods to detect nitric oxide and its metabolites in biological samples. Free Radical Biology & Medicine. 2007; 43: 645–657.
[40] Mansouri RA, Ahmed AM, Alshaibi HF, Al-Bazi MM, Banjabi AA, Alsufiani HM, *et al*. A new cirrhotic animal protocol combining carbon tetrachloride with methotrexate to address limitations of the currently used chemical-induced models. Frontiers in Pharmacology. 2023; 14: 1201583.
[41] Wang W, Hao X, Chen S, Yang Z, Wang C, Yan R, *et al*. pH-responsive Capsaicin@chitosan nanocapsules for antibiofouling in marine applications. Polymer. 2018; 158: 223–230.
[42] Thongin S, Den-Udom T, Uppakara K, Sriwantana T, Sibmooh N, Laolob T, *et al*. Beneficial effects of capsaicin and dihydrocapsaicin on endothelial inflammation, nitric oxide production and antioxidant activity. Biomedicine & Pharmacotherapy. 2022; 154: 113521.
[43] Feng Y, Zhu Y, Wan J, Yang X, Firempong CK, Yu J, *et*

al. Enhanced oral bioavailability, reduced irritation and increased hypolipidemic activity of self-assembled capsaicin prodrug nanoparticles. Journal of Functional Foods. 2018; 44: 137–145.

[44] Abukhalil MH, Althunibat OY, Aladaileh SH, Al-Amarat W, Obeidat HM, Al-Khawalde AAMA, *et al*. Galangin attenuates diabetic cardiomyopathy through modulating oxidative stress, inflammation and apoptosis in rats. Biomedicine & Pharmacotherapy. 2021; 138: 111410.

[45] Wang L, Zeng YQ, Gu JH, Song R, Cang PH, Xu YX, *et al*. Novel oral edaravone attenuates diastolic dysfunction of diabetic cardiomyopathy by activating the Nrf2 signaling pathway. European Journal of Pharmacology. 2022; 920: 174846.

[46] Popescu M, Chiutu L, Mircioiu C, Dima Ş. Capsaicin microemulsions: Preparation, characterization and *in vitro* release study. Farmacia. 2013; 62: 58–68.

[47] Herrmann H, Cabet E, Chevalier NR, Moosmann J, Schultheis D, Haas J, *et al*. Dual Functional States of R406W-Desmin Assembly Complexes Cause Cardiomyopathy With Severe Intercalated Disc Derangement in Humans and in Knock-In Mice. Circulation. 2020; 142: 2155–2171.

[48] Ma ZG, Yuan YP, Wu HM, Zhang X, Tang QZ. Cardiac fibrosis: new insights into the pathogenesis. International Journal of Biological Sciences. 2018; 14: 1645–1657.

[49] Aujla PK, Kassiri Z. Diverse origins and activation of fibroblasts in cardiac fibrosis. Cellular Signalling. 2021; 78: 109869.

[50] Venugopal H, Hanna A, Humeres C, Frangogiannis NG. Properties and Functions of Fibroblasts and Myofibroblasts in Myocardial Infarction. Cells. 2022; 11: 1386.

[51] Bachmann JC, Baumgart SJ, Uryga AK, Bosteen MH, Borghetti G, Nyberg M, *et al*. Fibrotic Signaling in Cardiac Fibroblasts and Vascular Smooth Muscle Cells: The Dual Roles of Fibrosis in HFpEF and CAD. Cells. 2022; 11: 1657.

[52] Ock S, Ham W, Kang CW, Kang H, Lee WS, Kim J. IGF-1 protects against angiotensin II-induced cardiac fibrosis by targeting αSMA. Cell Death & Disease. 2021; 12: 688.

[53] Burke RM, Burgos Villar KN, Small EM. Fibroblast contributions to ischemic cardiac remodeling. Cellular Signalling. 2021; 77: 109824.

[54] Shah AK, Bhullar SK, Elimban V, Dhalla NS. Oxidative Stress as A Mechanism for Functional Alterations in Cardiac Hypertrophy and Heart Failure. Antioxidants (Basel, Switzerland). 2021; 10: 931.

[55] Filardi T, Ghinassi B, Di Baldassarre A, Tanzilli G, Morano S, Lenzi A, *et al*. Cardiomyopathy Associated with Diabetes: The Central Role of the Cardiomyocyte. International Journal of Molecular Sciences. 2019; 20: 3299.

[56] Joubert M, Manrique A, Cariou B, Prieur X. Diabetes-related cardiomyopathy: The sweet story of glucose overload from epidemiology to cellular pathways. Diabetes & Metabolism. 2019; 45: 238–247.

[57] Domínguez-Martínez I, Meza-Márquez OG, Osorio-Revilla G, Proal-Nájera J, Gallardo-Velázquez T. Determination of capsaicin, ascorbic acid, total phenolic compounds and antioxidant activity of Capsicum annuum L. var. serrano by mid infrared spectroscopy (Mid-FTIR) and chemometric analysis. Journal of the Korean Society for Applied Biological Chemistry. 2014; 57: 133–142.

[58] Lavorgna M, Orlo E, Nugnes R, Piscitelli C, Russo C, Isidori M. Capsaicin in hot chili peppers: In vitro evaluation of its antiradical, antiproliferative and apoptotic activities. Plant Foods for Human Nutrition. 2019; 74: 164–170.

[59] Li Z, Zhang J, Cheng K, Zhang L, Wang T. Capsaicin alleviates the intestinal oxidative stress via activation of TRPV1/PKA/UCP2 and Keap1/Nrf2 pathways in heat-stressed mice. Journal of Functional Foods. 2023; 108: 105749.

[60] Funes SC, Rios M, Fernández-Fierro A, Covián C, Bueno SM, Riedel CA, *et al*. Naturally Derived Heme-Oxygenase 1 Inducers and Their Therapeutic Application to Immune-Mediated Diseases. Frontiers in Immunology. 2020; 11: 1467.

[61] Consoli V, Sorrenti V, Grosso S, Vanella L. Heme Oxygenase-1 Signaling and Redox Homeostasis in Physiopathological Conditions. Biomolecules. 2021; 11: 589.

[62] Jung HY, Kim DW, Yim HS, Yoo DY, Kim JW, Won MH, *et al*. Heme Oxygenase-1 Protects Neurons from Ischemic Damage by Upregulating Expression of Cu,Zn-Superoxide Dismutase, Catalase, and Brain-Derived Neurotrophic Factor in the Rabbit Spinal Cord. Neurochemical Research. 2016; 41: 869–879.

[63] Lee P, Greenfield JR. Non-pharmacological and pharmacological strategies of brown adipose tissue recruitment in humans. Molecular and Cellular Endocrinology. 2015; 418 Pt 2: 184–190.

[64] Song JX, Ren H, Gao YF, Lee CY, Li SF, Zhang F, *et al*. Dietary capsaicin improves glucose homeostasis and alters the gut microbiota in obese diabetic ob/ob mice. Frontiers in Physiology. 2017; 8: 602.

[65] Zheng J, Zheng S, Feng Q, Zhang Q, Xiao X. Dietary capsaicin and its anti-obesity potency: from mechanism to clinical implications. Bioscience Reports. 2017; 37: BSR20170286.

[66] Panchal SK, Bliss E, Brown L. Capsaicin in Metabolic Syndrome. Nutrients. 2018; 10: 630.

[67] Li W, Yang H, Lu Y. Capsaicin alleviates lipid metabolism disorder in high beef fat-fed mice. Journal of Functional Foods. 2019; 60: 103444.

[68] Jubaidi FF, Zainalabidin S, Taib IS, Hamid ZA, Budin SB. The Potential Role of Flavonoids in Ameliorating Diabetic Cardiomyopathy via Alleviation of Cardiac Oxidative Stress, Inflammation and Apoptosis. International Journal of Molecular Sciences. 2021; 22: 5094.

[69] Zheng X, Zhong T, Ma Y, Wan X, Qin A, Yao B, *et al*. Bnip3 mediates doxorubicin-induced cardiomyocyte pyroptosis via caspase-3/GSDME. Life Sciences. 2020; 242: 117186.

[70] Imanaka-Yoshida K. Inflammation in myocardial disease: From myocarditis to dilated cardiomyopathy. Pathology International. 2020; 70: 1–11.

[71] Nishida K, Otsu K. Inflammation and metabolic cardiomyopathy. Cardiovascular Research. 2017; 113: 389–398.

[72] Abbate A, Toldo S, Marchetti C, Kron J, Van Tassell BW, Dinarello CA. Interleukin-1 and the Inflammasome as Therapeutic Targets in Cardiovascular Disease. Circulation Research. 2020; 126: 1260–1280.

[73] Yue E, Yu Y, Wang X, Liu B, Bai Y, Yang B. Anthocyanin Protects Cardiac Function and Cardiac Fibroblasts from High-Glucose Induced Inflammation and Myocardial Fibrosis by Inhibiting IL-17. Frontiers in Pharmacology. 2021; 11: 593633.

[74] Zhang F, Li Y, Xin W, Wang L, Zhang Y, Xu H, *et al*. Gypenosides and capsaicinoids in combination ameliorates high-fat-diet-induced rat hyperlipidemia via the PPARγ-LXRα-ABCA1/ABCG1 pathway. Journal of Functional Foods. 2023; 108: 105714.

[75] Yoon S, Kim M, Min HK, Lee YU, Kwon DH, Lee M, *et al*. Inhibition of heat shock protein 70 blocks the development of cardiac hypertrophy by modulating the phosphorylation of histone deacetylase 2. Cardiovascular Research. 2019; 115: 1850–1860.

[76] Li R, Lan Y, Chen C, Cao Y, Huang Q, Ho CT, *et al*. Anti-obesity effects of capsaicin and the underlying mechanisms: a review. Food & Function. 2020; 11: 7356–7370.